

# Separated $\text{CoFe}_2\text{O}_4/\text{CoFe}$ nanoparticles by the $\text{SiO}_x$ matrix: revealing the intrinsic origin for the small remanence magnetization

B. Q. Geng · Y. Q. Ma · Y. F. Xu ·  
S. T. Xu · X. Sun · G. H. Zheng · Z. X. Dai

Received: 20 January 2015 / Accepted: 22 June 2015 / Published online: 1 July 2015  
© Springer Science+Business Media Dordrecht 2015

**Abstract** In order to clarify the intrinsic reason for the smaller remanence ( $M_r$ )-to-saturation ( $M_s$ ) magnetization ratio  $M_r/M_s$  than that expected by the Stoner–Wohlfarth model in  $\text{CoFe}_2\text{O}_4/\text{CoFe}_2$  nanoparticles in the previous report, we first prepared well-dispersed  $\text{CoFe}_2\text{O}_4$  nanoparticles, and then they were diluted in the  $\text{SiO}_2$  matrix followed by reduction in  $\text{H}_2$  as far as possible to exclude or reduce disadvantageous variables (such as the growth and aggregation of particles and the exchange coupling between soft magnetic particles in the process of reducing) affecting magnetic properties. Such an idea has not been taken into account before to our knowledge. The analyses on the magnetic results indicate that the  $\text{CoFe}_2\text{O}_4/\text{CoFe}_2$  nanoparticles herein reported are a pure dipolar system, in which the coercivity ( $H_c$ ) and  $M_r/M_s$  ratio are very sensitive to the anisotropy and the strength of dipolar interaction. These results signify that it is important to maintain the  $\text{CoFe}_2\text{O}_4/\text{CoFe}_2$  nanoparticles with higher anisotropy and weaker dipolar interaction for improving  $M_r/M_s$  and  $H_c$ . This suggestion was further confirmed by our another result wherein an  $M_r/M_s$  value of 0.64 was obtained even though no exchange coupling was observed in the

$\text{CoFe}_2\text{O}_4/\text{CoFe}_2$  nanoparticles, and further work is in process.

**Keywords** Thermal decomposition ·  $\text{CoFe}_2\text{O}_4/\text{CoFe}_2$  composite · Nanoparticles · Dipolar interaction · Anisotropy · Magnetism

## Introduction

Well-dispersed magnetic nanoparticles (NPs) have been widely investigated, because they not only possess unique properties differing from their bulk polycrystalline counterparts but also have potential applications in data storage and biotechnology. Furthermore, they provide a highly controlled experimental system for studying fundamental phenomena in physics (Coşkun et al. 2012; Topkaya et al. 2013; Xu et al. 2014a, b). Specially, nano-scaled  $\text{CoFe}_2\text{O}_4$  (CFO) NPs are very attractive because of their potentials in high-density information storage, electromagnetic wave absorption, ferrofluids, catalysts, drug targeting, magnetic separation, magnetic resonance imaging and gas sensor (Whitney et al. 1993; Carlà et al. 2013; Leite et al. 2012; Wu et al. 2011; Topkaya et al. 2013; Song and Zhang 2004). CFO is a cubic anisotropy crystal with the first crystalline anisotropy constant  $K_1 > 0$ , and therefore its theoretical remanence ( $M_r$ )-to-saturation ( $M_s$ ) ratio  $M_r/M_s$  is 0.832 in the case of noninteracting single domain particles with the randomly oriented easy axis

B. Q. Geng · Y. Q. Ma (✉) · Y. F. Xu ·  
S. T. Xu · X. Sun · G. H. Zheng · Z. X. Dai  
Anhui Key Laboratory of Information Materials and  
Devices, School of Physics and Materials Science, Anhui  
University, Hefei 230039, People's Republic of China  
e-mail: yqma@ahu.edu.cn

according to the Stoner–Wohlfarth model (Stoner and Wohlfarth 1948; Vargas et al. 2005). However, CFO has low  $M_s$  value because of its ferrimagnetism. Recently, numerous efforts have devoted to improve the values of  $M_s$  and  $M_r/M_s$  by compositing CFO with CoFe (CF) alloy.

Previously, the preparation of CFO/CF includes the synthesis of CFO and the subsequent reduction in the  $H_2$  ambience, aiming to achieve higher  $M_s$ ,  $M_r$ , and coercivity  $H_c$  values through exchange coupling between the hard and soft magnets. But almost all of the results give the following conclusions: (1) When the content of CF increases, the  $M_s$  value increases rapidly but is accompanied with a large loss of  $H_c$ . (2) In some previous reports, the exchange coupling between the hard and soft magnets was detected, but unfortunately the  $M_r/M_s$  ratio was not improved and even many reported  $M_r/M_s$  values were less than 0.5 (Quesada et al. 2014; Zan et al. 2013a, b, c; Li et al. 2015), the expected value theoretically for the uniaxial anisotropy crystal (Vargas et al. 2005). By carefully checking the results of the morphology characterizations in the previous reports, the following can be observed: (1) First of all, the prepared CFO particles aggregated seriously, and then they exhibited more severe conglomeration after they were reduced in the high-temperature condition. In such an undiluted or concentrated CFO/CF NP system, the exchange coupling effect may occur between hard/hard, hard/soft, and soft/soft grains, as shown in the schematic plot in

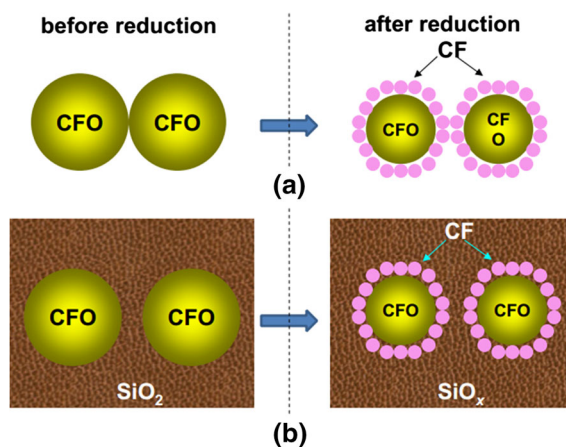


**Fig. 1** Schematic plots for the preparation of CFO/CF composites before and after reduction of  $CoFe_2O_4$  in the previous literature (a) and in this work (b)

Fig. 1a. It is possible that the detected exchange coupling in the previous reports occurs between the soft/soft CF grains because they remain in close contact after reduction, and such exchange coupling will be ineffective in improving  $M_r/M_s$ . (2) Besides the exchange coupling effect, the anisotropy also changes, because, on one hand, the relative content of hard and soft magnets varies with the reducing reaction, and on the other hand, reduction at high temperature gives rise to a change in the degree of aggregation and configuration which can be well understood with the results shown in Figs. 7, 9, 10 and 11 in our previous reports (Zan et al. 2013a, b, c). (3) In the concentrated or undiluted CFO/CF composite, the interparticle dipolar interaction cannot be neglected especially in the case of high content of soft CF with large  $M_s$  value because the dipolar field  $H_{dip}$  can be expressed as  $H_{dip} = 2 \mu/d^3$ , where  $\mu$  ( $\mu = M_s \times V$ ,  $V$  is the particle volume) is the average magnetic moment of magnetic particle and  $d$  is the distance between particles (center to center). Hence one can see that in the case of concentrated CFO/CF system the exchange coupling, anisotropy and dipolar interaction synergistically affect the magnetic properties, and such the system is unfit for revealing the intrinsic origin of the magnetic properties.

In this work, we first prepared well-dispersed CFO NPs, and then they were diluted in the  $SiO_2$  matrix, followed by reduction in  $H_2$  ambience in order to prevent magnetic NPs from aggregating during the process. This strategy has not been reported before as far as we know. The purposes of this strategy are as follows: (1) It can prohibit not only the agglomeration and growth of magnetic NPs but also the exchange coupling effect between soft CF particles as shown in Fig. 1b. (2) By changing the mass ratio of CFO/ $SiO_2$ , we can obtain magnetic NPs with different strengths of dipolar interactions. (3) By changing the reduction temperature, the relative content of CFO/CF can be altered, which consequently leads to the variation in anisotropy and dipolar interaction. Therefore such a system is a good model for studying the effect of dipolar interaction and anisotropy on magnetic properties. The results show that  $H_c$  and  $M_r$  are very sensitive to the dipolar interaction and anisotropy, making us understand that magnetic particles must be endowed with high anisotropy and weak dipolar interaction in order to improve the magnetic performance.

### Experimental procedures

The synthesis and characterization of CFO/SiO<sub>2</sub> were described elsewhere (Xu et al. 2015). The samples with the CFO/SiO<sub>2</sub> mass ratio of 50:50 and 5:95 are hereafter referred to as CFO50 and CFO5. The CFO50 and CFO5 samples were, respectively, reduced in the H<sub>2</sub> ambience (500 sccm, 96 % N<sub>2</sub> + 4 % H<sub>2</sub>) for 4 h at temperatures  $T_A = 300, 400, 500, 600, 700$  and 800 °C to obtain two groups of samples.

### Results and discussion

Crystal structures and morphology analysis of all samples

The crystal structures of all samples were characterized by the X-ray diffraction (XRD) method. Figures 2c–h, representatively, show the XRD patterns of samples CFO5 and CFO50 reduced at  $T_A = 300, 500$  and 700 °C. In the case of the CFO50 sample, it exhibits the pure cubic spinel CFO phase after reduction at 300 °C (Fig. 2c) according to the standard PDF card (Fig. 2a) of CoFe<sub>2</sub>O<sub>4</sub> (No. 22-1086). Subsequently, reduction at 500 °C distinctly weakens the diffraction intensity from CFO (Fig. 2d), and two additional clear diffraction peaks can be indexed to the diffraction from CF phase as compared with the PDF

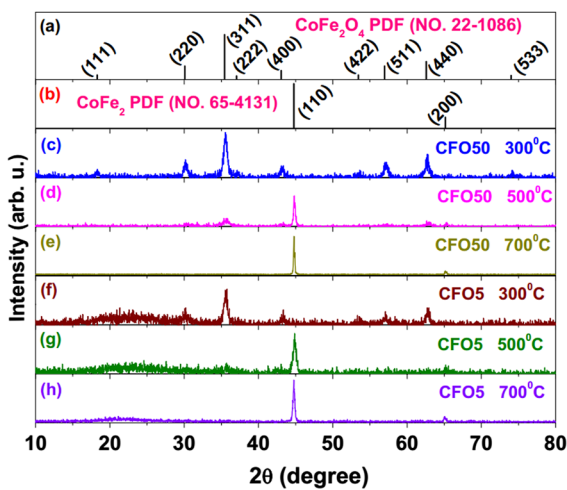


**Fig. 2** Standard PDF cards of CoFe<sub>2</sub>O<sub>4</sub> (No. 22-1086) (a) and CoFe<sub>2</sub> (No. 65-4131) (b); XRD patterns of samples CFO50 and CFO5 reduced at 300, 500 and 700 °C (c–h)

card of CoFe<sub>2</sub> (No. 65-4131) in Fig. 2b (Xiang et al. 2013). After reduction at 700 °C, the diffraction from CFO cannot be detected and the sample exhibits the pure CF phase (Fig. 2e) due to the reduction reaction:  $\text{CoFe}_2\text{O}_4 + 14\text{H}_2 \rightarrow \text{CoFe}_2 + 4\text{H}_2\text{O}$ . In the case of the sample CFO5, as shown in Figs. 2f–h, the phase evolves in the same trend as in the sample CFO50 except that the broad peak below  $2\theta = 30^\circ$  results from the amorphous SiO<sub>2</sub> (Nadeem et al. 2014). Figure 3 shows the normalized diffraction intensities from CFO (311) and CF (110) for the samples CFO50 (a) and CFO5 (b), more distinctly illustrating the phase evolution with the reducing temperature  $T_A$ .

The cell lattice parameter  $a$  of CFO and CF can be obtained from  $\sin^2\theta = \lambda^2(H^2 + K^2 + L^2)/4a^2$ , where  $\theta$  is the diffraction angle,  $\lambda$  the wavelength of the Cu  $K\alpha$  irradiation, and  $(HKL)$  the crystal plane index. The obtained lattice parameter  $a$  is equal to 0.838 and 0.287 nm, so the X-ray density is calculated to be 5.43 and 8.03 g/cm<sup>3</sup> for CFO and CF, respectively.

Figure 4a shows the low-magnification TEM image of the as-prepared CoFe<sub>2</sub>O<sub>4</sub> with the inset being the TEM image for the sample CFO5. The as-prepared CoFe<sub>2</sub>O<sub>4</sub> is composed of well-dispersed NPs. For the CFO5 sample, the TEM image is not so clear as that for the as-prepared CoFe<sub>2</sub>O<sub>4</sub> sample because CoFe<sub>2</sub>O<sub>4</sub> NPs in the CFO5 sample were highly diluted by the amorphous SiO<sub>2</sub> matrix. The particle size histogram and the Gaussian-fitting curve (solid line) are shown in Fig. 4b, giving the particle size of  $16.3 \pm 4$  nm. In the case of the sample CFO50 after reduction at 500 °C, the high-resolution transmission electron microscopy

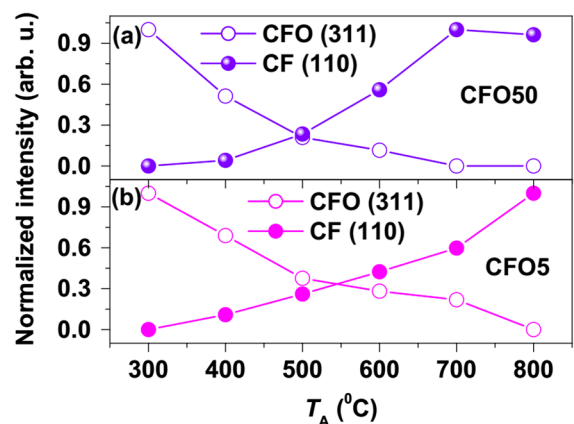


**Fig. 3** The normalized diffraction intensities from CFO (311) and CF (110) for the samples CFO50 (a) and CFO5 (b)

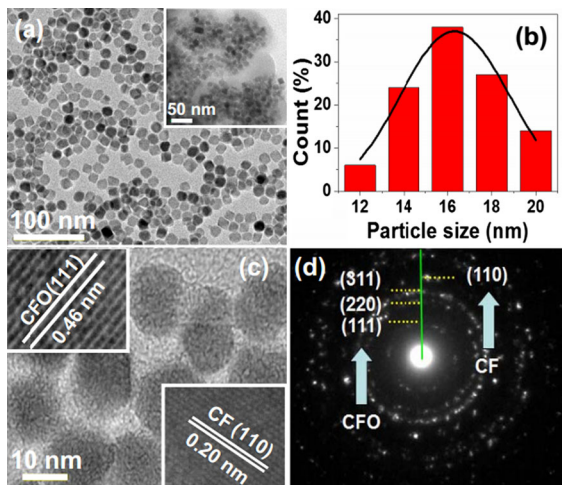


**Fig. 4** The low-magnification TEM image of the as-prepared CFO (a) with the *inset* being the TEM image of the CFO5 sample; the particle size histogram and the Gaussian-fitting curve (*solid line*) (b); the HRTEM image (c) with the magnified details of fringes corresponding to the CFO (111) (*upper-left inset*) and CF (110) (*lower-right inset*) crystalline planes, and the SAED image (d) for the CFO50 reduced at 500 °C

(HRTEM) (Fig. 4c) shows that CFO/CF NPs are separated from each other even though they are treated at 500 °C due to the isolation of SiO<sub>2</sub> matrix, which is different from the previous results in literature; the upper-left and lower-right insets show the magnified details of fringes of the CFO (111) and CF (110) crystalline planes, respectively, indicating the formation of CFO/CF composite; in these isolated NPs, at least the exchange interaction between CF grains, which is a short-range one in nature, can be excluded. Figure 4d shows the selected area electron diffraction (SAED) pattern of CFO50 reduced at 500 °C, also illustrating the formation of the composite.

#### The magnetic properties

Figure 5 shows the magnetization ( $M$ ) dependence on the applied magnetic field ( $H$ ) ( $-40 \text{ kOe} < H < +40 \text{ kOe}$ ) measured at room temperature, i.e.  $M(H)$  loops of the CFO5 samples reduced at different temperatures from 300 to 800 °C. The magnetic parameters, including  $H_c$ ,  $M_s$  as well as  $M_r/M_s$  drawn from loops, are listed in Table 1. The sample reduced at 300 °C, almost the pure CFO as shown in Fig. 2, has the largest  $H_c$  (2321 Oe) and  $M_r/M_s$  (0.46) values but the smallest  $M_s$  (18.04 emu/g)

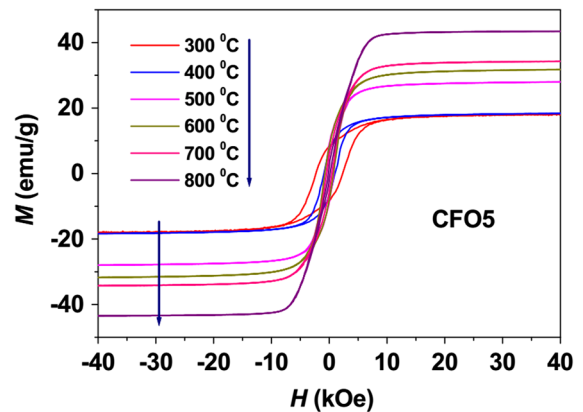


**Fig. 5** The magnetization ( $M$ ) dependence on the applied magnetic field ( $H$ ) ( $-4 \text{ T} < H < +4 \text{ T}$ ) measured at room temperature, viz  $M(H)$  loops of the CFO5 samples reduced at different temperatures from 300 to 800 °C

**Table 1** Magnetic parameters of the CF5 samples reduced at different temperatures

$T_A$ (°C)	$H_c$ (Oe)	$M_s$ (emu/g)	$M_r/M_s$
300	2321	18.04	0.46
400	923	18.37	0.37
500	761	27.99	0.32
600	763	31.75	0.26
700	456	34.22	0.17
800	169	43.44	0.05

value. Upon increasing  $T_A$  to 800 °C, both  $H_c$  and  $M_r/M_s$  decrease monotonously to 169 Oe and 0.05, which vary in the same trend as reported before (Soares et al. 2011), while  $M_s$  increases to 43.44 emu/g. These behaviors phenomenally can be assigned to the increase of CF phase and the intrinsic origin will be further discussed below.

Figure 6 shows the room temperature  $M(H)$  loops of the CFO50 samples reduced at different temperatures from 300 to 800 °C. The loops exhibit similar characteristics as shown in Fig. 5. The values of  $H_c$ ,  $M_s$ , and  $M_r/M_s$  are listed in Table 2. These parameters change with  $T_A$  in the same trend as occurred in the sample CFO5. The  $M_s$  value is obviously greater than that for the sample CFO5 because of the higher concentration of magnetic NPs, and the highest  $M_s$  value of 183.80 emu/g is attained after reduction at 700 °C.

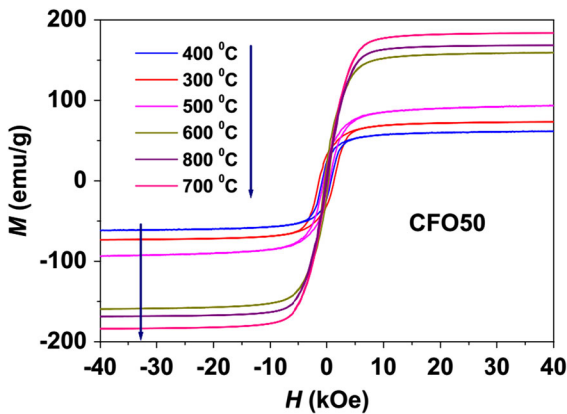


**Fig. 6**  $M(H)$  loops of the CFO50 samples reduced at different temperatures from 300 to 800 °C

**Table 2** Magnetic parameters of the CF50 samples reduced at different temperatures

$T_A$ (°C)	$H_c$ (Oe)	$M_s$ (emu/g)	$M_r/M_s$
300	1368	73.33	0.43
400	791	61.64	0.38
500	556	93.52	0.23
600	331	159.40	0.13
700	146	183.80	0.04
800	136	168.58	0.04

Analysis on the magnetic properties

*The anisotropy field  $H_K$*

As reported before (Laureti et al. 2010), the splitting point, where the magnetizing and demagnetizing branches separate ( $\Delta M$ ), corresponds to the irreversibility field which can be regarded as an estimate of anisotropy field  $H_K$ . Herein  $H_K$  is artificially regulated to be the magnetic field corresponding to the splitting point, where  $\Delta M/M_s$  is equal to 5 %. The obtained  $H_K$  values for the CFO50 (solid circles) and CFO5 (empty circles) are shown in Fig. 7. With the increasing  $T_A$ , they both decrease monotonously, and the reasons are as follows: (1) The increase of CoFe<sub>2</sub> phase enhances the  $M_s$  value, because CoFe<sub>2</sub> is a typical soft ferromagnetic material with a high  $M_s$  value of about 230 emu/g (Mohan et al. 2008), consequently diminishing the  $H_K$  value due to  $H_K = 2K/M_s$ , where  $K$  is the effective anisotropy

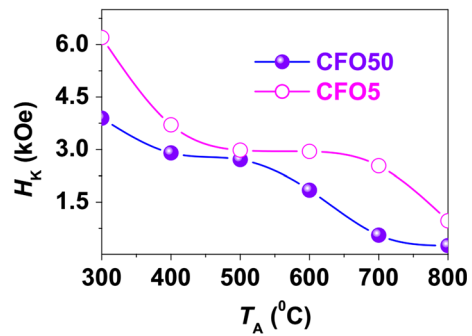


**Fig. 7** The anisotropy field  $H_K$  of the CFO50 and CFO5 samples reduced at different temperatures

constant. (2) For the soft and hard composite system, the effective anisotropy constant  $K$  is expressed by  $K = f_s K_s + f_h K_h$ , where  $f_s$  and  $f_h$  are the volume fraction, and  $K_s$  and  $K_h$  are anisotropy constant of soft and hard phases with  $K_s \ll K_h$ , respectively (Skomski and Coey 1993). The increase of  $T_A$  raises the volume fraction  $f_s$  of the soft magnetic CoFe<sub>2</sub> phase, diminishing the  $K$  value and consequently resulting in the decrease of  $H_K$ . Additionally the  $H_K$  of CFO50 is smaller than that of CFO5, partially because CFO50 has a higher  $M_s$  value.

*The dipolar field  $H_{dip}$*

To test the interactions between the grains, the  $\delta m$  curves were measured. The  $\delta m$  curves were built using the magnetizing  $M_r(H)$  and demagnetizing  $M_d(H)$  remanent magnetizations. The measuring methods of  $M_r(H)$  and  $M_d(H)$  are identical with those reported in reference (Soares et al. 2011).  $M_r(H)$  and  $M_d(H)$  are normalized by the saturation remanence  $M_r(H_{sat})$ :  $m_r(H) = M_r(H)/M_r(H_{sat})$  and  $m_d(H) = M_d(H)/M_d(H_{sat})$ , where  $H_{sat}$  is an applied field to saturate the magnetization, and the  $\delta m$  is expressed as  $\delta m(H) = m_d(H) - [1 - 2m_r(H)]$ . Figure 8 representatively shows the  $\delta m$  curves of the samples CFO50 and CFO5 reduced at 300, 500, and 800 °C. Several main points are summarized as follows: (1) All  $\delta m$  curves exhibit the negative peak. The negative peak is an evidence of the predominance of dipole–dipole interactions, while the positive peak can be attributed to the predominance of exchange interactions. The  $\delta m$  plots indicate that the thermal treatments up to 800 °C do not induce exchange coupling between particle surfaces due to the isolation of SiO<sub>2</sub>, or in other words



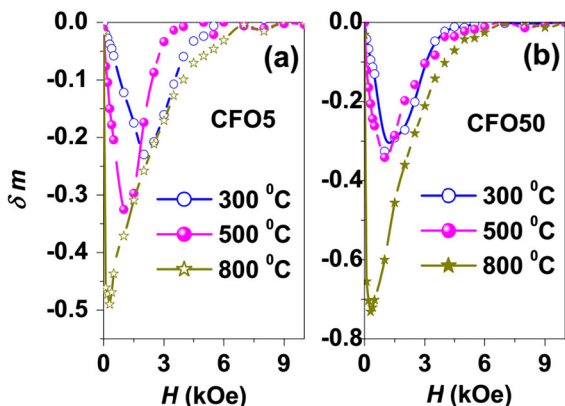


**Fig. 8** The  $\delta m$  curves of CFO5 (a) and CFO50 (b) samples reduced at temperatures of 300, 500 and 800 °C

all samples are pure dipolar systems. (2) The  $\delta m$  amplitudes (i.e. strength of interparticle interactions) are 0.23, 0.33, and 0.49 for the CFO5 samples, and 0.33, 0.34, and 0.73 for the CFO50 samples reduced at 300, 500, and 800 °C, respectively. These data suggest that reduction at higher temperature enhances the strength of interparticle dipolar interactions. (3) The  $\delta m$  amplitudes of the CFO5 samples are smaller than those of the corresponding CFO50 samples, because the concentration (average distance) of  $\text{CoFe}_2\text{O}_4$  NPs is smaller (longer) in the CFO5 samples. These conclusions can be better understood by analyzing the dipolar field, as discussed below.

In a sample of randomly distributed NPs with average magnetic moment  $\mu$  ( $\mu = M_s \times V$ ,  $V$  is the particle volume), the maximum dipolar field  $H_{\text{dip}}$  between nearest-neighboring particles is  $H_{\text{dip}} = 2 \mu / d^3$ , where  $d$  is the distance between particles (center to center). The  $H_{\text{dip}}$  curves are shown in Fig. 9. It can be noticed that (1) after reduction above 500 °C,  $H_{\text{dip}}$  increases rapidly resulting from the increase of  $\mu$  due to the appearance of  $\text{CoFe}_2$  phase, and (2) the  $H_{\text{dip}}$  values of CFO50 samples are higher than those of the CFO5 samples because of the smaller  $d$  and larger  $M_s$  in CFO50 samples.

Figure 10 shows the  $H_K$  and  $H_{\text{dip}}$  for the samples CFO5 (a) and CFO50 (b). In the case of CFO5 samples,  $H_K$  is larger than  $H_{\text{dip}}$  at all reducing temperatures, suggesting that anisotropy dominates the magnetic properties because the  $\text{CoFe}_2\text{O}_4$  NPs are highly diluted in the  $\text{SiO}_x$  matrix, leading to the weak dipolar interaction. In the case of CFO50 samples,  $H_K$

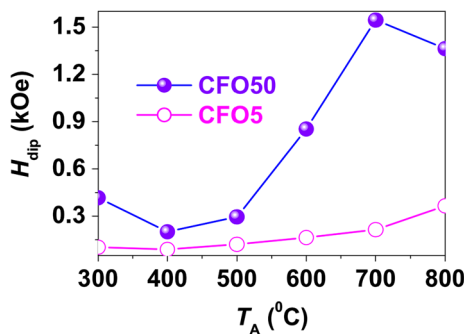


**Fig. 9** The maximum dipolar field  $H_{\text{dip}}$  of the CFO50 (solid circles) and CFO5 (empty circles) samples reduced at different temperatures

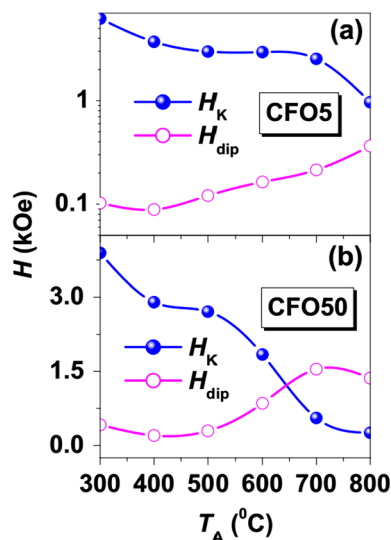


**Fig. 10** Comparison of  $H_K$  with  $H_{\text{dip}}$  in the samples CFO5 (a) and CFO50 (b)

is larger than  $H_{\text{dip}}$  as  $T_A \leq 600$  °C but  $H_K < H_{\text{dip}}$  as  $T_A > 600$  °C, suggesting that the dipolar interaction becomes the non-negligible energy to affect magnetic properties in samples reduced at  $T_A > 600$  °C.

#### Effects of dipolar interaction and anisotropy on the magnetic properties

As shown in Fig. 11a, for both the CFO5 and CFO50 samples,  $H_c$  monotonously decreases with the increasing  $T_A$ , but the underlying mechanism is somewhat different in both the samples. In the CFO5 samples with  $H_K \gg H_{\text{dip}}$  at all  $T_A$  values, the decrease in  $H_c$

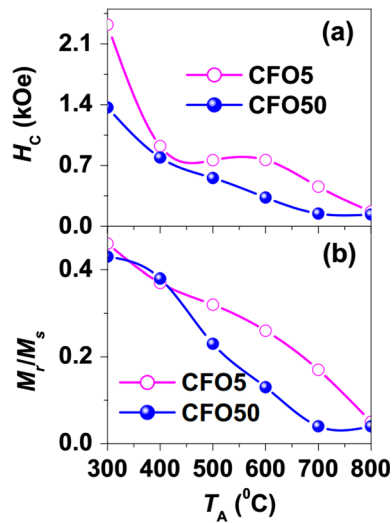


**Fig. 11** The  $H_c$  (a) and the  $M_r/M_s$  ratio (b) of the samples CFO5 (empty circles) and CFO50 (solid circles) samples

can be assigned to the decrease of  $H_K$  with  $T_A$  due to the appearance of soft magnetic  $\text{CoFe}_2$  alloys, as discussed in Fig. 10a. In the sample CFO50, the  $H_c$  is determined by anisotropy at  $T_A \leq 600$  °C and the synergistic effect between the anisotropy and the dipolar interaction at  $T_A > 600$  °C based on the discussion for Fig. 10b. Additionally, the  $H_c$  value of the CFO50 sample is less than that of the CFO5 sample, mainly because CFO50 has the smaller  $H_K$  value (Fig. 7) than CFO5.

The  $M_r/M_s$  ratios of the samples CFO5 (empty circles) and CFO50 (solid circles) are shown in Fig. 11b. They both monotonously decrease with the increasing  $T_A$ , which can be assigned to the synergistic effect of dipolar interaction and the anisotropy because the  $M_r/M_s$  ratio will be suppressed by increasing  $H_{\text{dip}}$  (Zan et al. 2013a, b, c; Xu et al. 2015; Zan et al. 2013a, b, c) or decreasing  $H_K$  (Xu et al. 2014a, b; Kurtan et al. 2013). Therefore, it is important to control the anisotropy and dipolar interaction for improving the  $M_r/M_s$  ratio. In order to support this viewpoint, the  $\text{CoFe}_2\text{O}_4$  NPs with the size of about 30 nm were prepared, as shown in the TEM image in Fig. 12a. After reduction at 300 °C for 1.5 h, the  $M(H)$  loop of the sample was measured, as shown in Fig. 12b. A high  $M_r/M_s$  ratio (0.64) above 0.5 and a high  $H_c$  value of 1660 Oe were obtained in the sample, even though exchange coupling was not observed in the  $\delta m$  curve (not shown here), which can be assigned

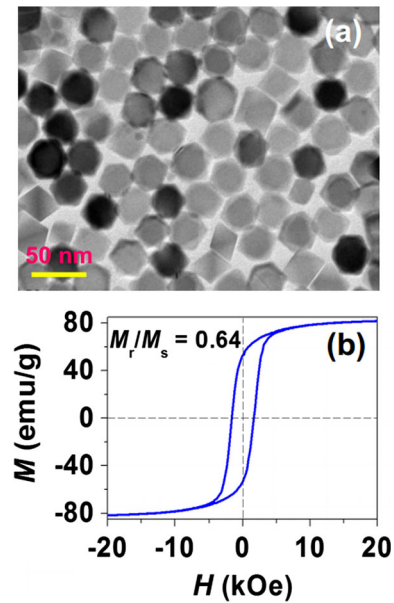


**Fig. 12** The TEM image of the undiluted  $\text{CoFe}_2\text{O}_4$  NPs (a) and the  $M(H)$  loop (b) of the sample after  $\text{CoFe}_2\text{O}_4$  was reduced at 300 °C for 1.5 h

to the high  $H_K$  (3615 Oe) and weak  $H_{\text{dip}}$  ( $\sim 230$  Oe) values, and further work is in process.

## Conclusions

The  $\text{CoFe}_2\text{O}_4$  NPs were synthesized by thermal decomposition of  $\text{Fe}(\text{acac})_3$  and  $\text{Co}(\text{acac})_2$ . The as-prepared  $\text{CoFe}_2\text{O}_4$  NPs exhibit good dispersity and uniform size of  $16.3 \pm 4$  nm. Then the  $\text{CoFe}_2\text{O}_4$  NPs were dispersed in the  $\text{SiO}_2$  matrix with different concentrations of 5 % (CFO5) and 50 % (CFO50), followed by subsequently reducing in the 4 %  $\text{H}_2 + 96$  %  $\text{N}_2$  ambience at different reducing temperatures,  $T_A$ , of 300, 400, 500, 600, 700 and 800 °C to obtain the composite of hard  $\text{CoFe}_2\text{O}_4$  and soft  $\text{CoFe}_2$  alloys, in order to change the anisotropy and the interparticle dipolar interaction. The anisotropy and the dipolar interaction in the CFO5 and CFO50 samples were compared in detail, and their effects on the magnetic properties of  $\text{CoFe}_2\text{O}_4/\text{CoFe}_2$  composite were discussed on which much attention has not been paid before. Several suggestions are as follows:

(1) The reasons for the smaller  $M_r/M_s$  ratio in the  $\text{CoFe}_2\text{O}_4/\text{CoFe}_2$  composite than 0.5 in the previous reports can be assigned to the weak anisotropy and/or

strong dipolar interaction in the concentrated magnetic NPs.

(2) The  $M_r/M_s$  ratio was not improved even if the exchange coupling was observed in undiluted  $\text{CoFe}_2\text{O}_4/\text{CoFe}_2$  composite, in which the exchange coupling maybe occurs between  $\text{CoFe}_2$  particles instead of between hard  $\text{CoFe}_2\text{O}_4$  and soft  $\text{CoFe}_2$  phases.

(3) In order to improve the  $H_c$  and  $M_r/M_s$  values, several important factors were suggested as follows: preparing the  $\text{CoFe}_2\text{O}_4$  particles with a suitable size for controlling the anisotropy; keeping the  $\text{CoFe}_2\text{O}_4$  particles separated from each other for controlling the strength of the dipolar interaction; preventing magnetic particles from conglomerating in the process of reducing to prepare  $\text{CoFe}_2\text{O}_4/\text{CoFe}_2$  composite.

We also suggest that the  $M_r/M_s$  ratio can be further increased if the exchange coupling between hard and soft magnets can be successfully accomplished. Further related work is in process.

**Acknowledgments** This work was supported by the National Natural Science Foundation of China (Grant Nos. 11174004 and 51471001).

## References

- Carlà F, Campo G, Sangregorio C, Caneschi A, Fernández CDJ, Cabrera LI (2013) Electrochemical characterization of core@shell  $\text{CoFe}_2\text{O}_4/\text{Au}$  composite. *J Nanopart Res* 15:1813
- Coşkun M, Can MM, Coşkun ÖD, Korkmaz M, Firat T (2012) Surface anisotropy change of  $\text{CoFe}_2\text{O}_4$  nanoparticles depending on thickness of coated  $\text{SiO}_2$  shell. *J Nanopart Res* 14:1197
- Kurtan U, Topkaya R, Baykal A (2013) Sol-gel auto-combustion synthesis of PVP/ $\text{CoFe}_2\text{O}_4$  nanocomposite and its magnetic characterization. *Mater Res Bull* 48:4889–4895
- Lauretì S, Varvaro G, Testa AM, Fiorani D, Agostinelli E, Piccaluga G et al (2010) Magnetic interactions in silica coated nanoporous assemblies of  $\text{CoFe}_2\text{O}_4$  nanoparticles with cubic magnetic anisotropy. *Nanotechnology* 21:315701
- Leite GCP, Chagas EF, Pereira R, Prado RJ, Terezo AJ, Alzamora M, Baggio-Saitovitch E (2012) Exchange coupling behavior in bimagnetic  $\text{CoFe}_2\text{O}_4/\text{CoFe}_2$  nanocomposite. *J Magn Magn Mater* 324:2711–2716
- Li WX, Wang LC, Li GM, Xu Y (2015) Hollow  $\text{CoFe}_2\text{O}_4-\text{Co}_3\text{Fe}_7$  microspheres applied in electromagnetic absorption. *J Magn Magn Mater* 377:259–266
- Mohan M, Chandra V, Manoharan SS (2008) A new nano  $\text{CoFe}_2$  alloy precursor for cobalt ferrite production via sono-reduction process. *Curr Sci India* 94:473–476
- Nadeem K, Krenn H, Sarwar W, Mumtaz M (2014) Comparison of surface effects in  $\text{SiO}_2$  coated and uncoated nickelferrite nanoparticles. *Appl Surf Sci* 288:677–681
- Quesada A, Rubio-Marcos F, Marco JF, Mompean FJ, García-Hernández M, Fernández JF (2014) On the origin of remanence enhancement in exchange-uncoupled  $\text{CoFe}_2\text{O}_4$ -based composites. *Appl Phys Lett* 105:202405
- Skomski R, Coey JMD (1993) Giant energy product in nanostructured two-phase magnets. *Phys Rev B* 48:15812
- Soares JM, Cabral FAO, Araújo JHD, Machado FLA (2011) Exchange-spring behavior in nanopowders of  $\text{CoFe}_2\text{O}_4-\text{CoFe}_2$ . *Appl Phys Lett* 98:072502
- Song Q, Zhang ZJ (2004) Shape control and associated magnetic properties of spinel cobalt ferrite nanocrystals. *J Am Chem Soc* 126:6164–6168
- Stoner EC, Wohlfarth EP (1948) A mechanism of magnetic hysteresis in heterogeneous alloys. *Philos Trans R Soc Lond A* 240:599–642
- Topkaya R, Baykal A, Demir A (2013) Yafet-Kittel-type magnetic order in Zn-substituted cobalt ferrite nanoparticles with uniaxial anisotropy. *J Nanopart Res* 15:1359
- Vargas JM, Nunes WC, Socolovsky LM, Knobel M, Zanchet D (2005) Effect of dipolar interaction observed in iron-based nanoparticles. *Phys Rev B* 72:184428
- Whitney TM, Searson PC, Jiang JS, Chien CL (1993) Fabrication and magnetic properties of arrays of metallic nanowires. *Science* 261:1316–1319
- Wu HX, Liu G, Wang X, Zhang JM, Chen Y, Shi JL, Yang H, Hu H, Yang SP (2011) Solvothermal synthesis of cobalt ferrite nanoparticles loaded on multiwalled carbon nanotubes for magnetic resonance imaging and drug delivery. *Acta Biomater* 7:3496–3504
- Xiang J, Zhang XH, Li JL, Chu YQ, Shen XQ (2013) Fabrication, characterization, exchange coupling and magnetic behavior of  $\text{CoFe}_2\text{O}_4/\text{CoFe}_2$  nanocomposite nanofibers. *Chem Phys Lett* 576:39–43
- Xu ST, Ma YQ, Xu YF, Sun X, Geng BQ, Zheng GH, Dai ZX (2014a) The effects of surface spin on magnetic properties of weak magnetic  $\text{ZnLa}_{0.02}\text{Fe}_{1.98}\text{O}_4$  nanoparticles. *Nanoscale Res Lett* 9:545
- Xu YF, Ma YQ, Xu ST, Zan FL, Zheng GH, Dai ZX (2014b) Obtainment of exchange coupling coefficient of  $\text{Ni}_{0.6}\text{Zn}_{0.4}\text{Fe}_2\text{O}_4/\text{SrFe}_{12}\text{O}_{19}$  composites. *Mater Lett* 131:203–205
- Xu ST, Ma YQ, Xu YF, Sun X, Geng BQ, Zheng GH, Dai ZX (2015) Pure dipolar-interacted  $\text{CoFe}_2\text{O}_4$  nanoparticles and their magnetic properties. *Mater Res Bull* 62:142–147
- Zan FL, Ma YQ, Ma Q, Xu YF, Dai ZX, Zheng GH, Wu MZ, Li G (2013a) Magnetic and impedance properties of nanocomposite  $\text{CoFe}_2\text{O}_4/\text{Co}_{0.7}\text{Fe}_{0.3}$  and single-phase  $\text{CoFe}_2\text{O}_4$  prepared via One-step hydrothermal synthesis. *J Am Ceram Soc* 96:3100–3107
- Zan FL, Ma YQ, Ma Q, Xu YF, Dai ZX, Zheng GH (2013b) Giant exchange bias and exchange enhancement observed in  $\text{CoFe}_2\text{O}_4$ -based composites. *J Alloy Compd* 581:263–269
- Zan FL, Ma YQ, Ma Q, Zheng GH, Dai ZX, Wu MZ, Li G, Sun ZQ, Chen XS (2013c) One-step hydrothermal synthesis and characterization of high magnetization  $\text{CoFe}_2\text{O}_4/\text{Co}_{0.7}\text{Fe}_{0.3}$  nanocomposite permanent magnets. *J Alloy Compd* 553:79–85